**Atmospheric
Chemistry
and Physics
Discussions**

Ozone production in remote oceanic and industrial areas derived from ship based measurements of peroxy radicals during TexAQS 2006

R. Sommariva[1,2,*], S. S. Brown[1], J. M. Roberts[1], D. M. Brookes[3,**],
A. E. Parker[3,***], P. S. Monks[3], T. S. Bates[4], D. Bon[1,2], J. A. de Gouw[1,2],
G. J. Frost[1,2], J. B. Gilman[1,2], P. D. Goldan[1,2], S. C. Herndon[5], W. C. Kuster[1,2],
B. M. Lerner[1,2], H. D. Osthoff[1,2,****], S. C. Tucker[1,2,*****], C. Warneke[1,2],
E. J. Williams[1,2], and M. S. Zahniser[5]

[1]Earth System Research Laboratory, NOAA, Boulder, CO, USA
[2]CIRES, University of Colorado, Boulder, CO, USA
[3]Department of Chemistry, University of Leicester, Leicester, UK
[4]Pacific Marine Environmental Laboratory, NOAA, Seattle, WA, USA
[5]Aerodyne Research, Inc., Billerica, MA, USA
[*]now at: School of Environmental Sciences, University of East Anglia, Norwich, UK

Discussion Paper | Discussion Paper | Discussion Paper | Discussion Paper

ACPD

10, 23109–23147, 2010

**RO$_2$ measurements
and O$_3$ production
during TexAQS 2006**

R. Sommariva et al.

Title Page

Abstract | Introduction

Conclusions | References

Tables | Figures

◄◄ | ►►

◄ | ►

Back | Close

Full Screen / Esc

Printer-friendly Version

Interactive Discussion

**now at: Air Quality Practice, AEA plc., Harwell, Didcot, UK
***now at: PC2A, Université des Sciences et Technologies de Lille, Lille, France
****now at: Department of Chemistry, University of Calgary, Calgary, Canada
*****now at: Ball Aerospace & Technologies Corp., Boulder, CO, USA

Correspondence to: R. Sommariva (r.sommariva@uea.ac.uk)

Title Page

Abstract	Introduction
Conclusions	References
Tables	Figures

|◄ | ►|
◄ | ►

Back | Close

Full Screen / Esc

Printer-friendly Version

Interactive Discussion

Abstract

During the Texas Air Quality Study II (TexAQS 2006) campaign, a PEroxy Radical Chemical Amplifier (PERCA) was deployed on the NOAA research vessel R/V *Brown* to measure total peroxy radicals (HO$_2$+ΣRO$_2$). Day-time mixing ratios of HO$_2$+ΣRO$_2$

5 between 25 and 110 ppt were observed throughout the study area – the Houston/Galveston region and the Gulf coast of the U.S. – and analyzed in relation to measurements of nitrogen oxides, volatile organic compounds (VOC) and photolysis rates to assess radical sources and sinks in the region.

The measurements of HO$_2$+ΣRO$_2$ were used to calculate the in-situ net photochem-

10 ical formation of ozone. Measured median values ranged from 0.6 ppb/h in clean oceanic air masses up to several tens of ppb/h in the most polluted industrial areas. The results are consistent with previous studies and generally agree with observations made during the previous TexAQS 2000 field campaign. The net photochemical ozone formation rates determined at Barbours Cut, a site immediately south of the Houston

15 Ship Channel, were analyzed in relation to local wind direction and VOC reactivity to understand the relationship between ozone formation and local VOC emissions.

The measurements of HO$_2$+ΣRO$_2$ made during the R/V *Brown* TexAQS 2006 cruise indicate that ozone formation is NO$_x$-limited in the Houston/Galveston region and influenced by highly reactive hydrocarbons, especially alkenes from urban and industrial

20 sources and their photooxidation products, such as formaldehyde.

1   Introduction

Peroxy radicals (HO$_2$ and RO$_2$) are crucial intermediates in the photochemical formation of ozone (O$_3$) in the lower atmosphere because they drive the conversion between NO and NO$_2$ that leads to net ozone production (Reactions R1–R4).

25   $RO_2 + NO \rightarrow RO + NO_2$ (R1)

$$NO_2 + h\nu \rightarrow NO + O(^3P) \qquad (\lambda < 420 \text{ nm}) \qquad \text{(R2)}$$

$$O(^3P) + O_2 \ (+M) \rightarrow O_3 \ (+M) \qquad \text{(R3)}$$

$$NO + O_3 \rightarrow NO_2 + O_2 \qquad \text{(R4)}$$

Peroxy radicals are formed from the oxidation of carbon monoxide (CO) and a wide range of Volatile Organic Compounds (VOC). Oxidation of VOC is initiated in the troposphere by free radicals (OH, NO_3, Cl) and by ozone (Monks, 2005). Figure 1 illustrates the chemistry of the simplest peroxy radicals (HO_2, CH_3O_2, $C_2H_5O_2$ and CH_3CO_3) under high NO_x conditions. At low NO_x, peroxy radical self-reactions and reactions with O_3 act as net chemical sinks for ozone. Photochemical ozone formation can therefore be described in terms of peroxy radicals and NO concentrations. The only inorganic peroxy radical is HO_2, but there is a very large number of organic peroxy radicals (RO_2) owing to the variety of VOC emitted in the troposphere by natural and anthropogenic sources.

Total peroxy radical concentrations ($HO_2 + \Sigma RO_2$) were measured on board the NOAA research ship R/V *Brown* during a field campaign along the Gulf coast of the United States that took place in summer 2006 as part of the Second Texas Air Quality Study (Parrish et al., 2009). These measurements were then used to characterize the radical sources and sinks, their diurnal variation and the regional photochemistry relevant to ozone formation along the U.S. Gulf Coast.

Measurements of peroxy radicals from a mobile platform such as a ship provide a unique picture of radical chemistry across a wide range of environments. The R/V *Brown* sampled air from the remote Gulf of Mexico, aged urban pollution advected over water, highly polluted air from industrial areas associated with petrochemical facilities along the Gulf Coast and air influenced primarily by emissions from shipping. Measurements of peroxy radicals, in combination with nitrogen oxides, ozone and related compounds can provide a direct measurement of photochemical ozone production rates. These data show the regional variation in ozone production from clean to highly polluted areas and the correlation of these rates with specific pollutant types.
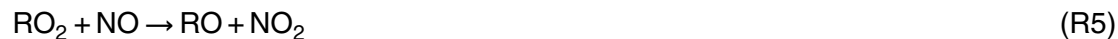
The instruments relevant to this work and the field campaign are described in Sect. 2. The measurements of $HO_2 + \Sigma RO_2$ are discussed in Sect. 3 and the photochemical formation of O_3 in Sect. 4. Throughout this paper, times are expressed in Greenwich Mean Time (GMT = local time + 5 h along the Gulf coast and GMT = local time + 4 h along the Atlantic Coast, Fig. 5).

2 Experimental

2.1 PERCA

Total peroxy radicals ($HO_2 + \Sigma RO_2$) were measured on the R/V *Brown* using a dual-channel PEroxy Radical Chemical Amplification (PERCA) from the University of Leicester, UK. The instrument has been used in several field studies and has been described in detail in previous publications (Monks et al., 1998; Salisbury et al., 2002; Fleming et al., 2006; Green et al., 2006; Parker et al., 2009).

The chemical amplification technique catalytically converts HO_2 and RO_2 into CO_2 and NO_2 (Cantrell et al., 1984, 1996). Organic peroxy radicals are converted into HO_2 (Reactions R5–R6) and HO_2 is converted into OH by reaction with NO (Reaction R7); by adding CO to the inlet, OH is converted back to HO_2 (Reaction R8), thus producing multiple NO_2 molecules per each HO_2 and RO_2 radical. NO_2 is then measured by luminol chemiluminescence. The amplification cycle is terminated when radicals are removed from the system, by formation of HONO, HNO_3, HO_2NO_2 or by loss on the inlet walls. The number of cycles before termination occurs is the chain length (*CL*), which is characteristic of the inlet and a measure of the efficiency of the amplification.

$$RO_2 + NO \rightarrow RO + NO_2 \tag{R5}$$

$$RO + O_2 \rightarrow HO_2 + RCHO \tag{R6}$$

$$HO_2 + NO \rightarrow OH + NO_2 \tag{R7}$$

$$OH + CO + O_2 \ (+M) \rightarrow HO_2 + CO_2 \ (+M) \tag{R8}$$

In addition to NO_2 formed by peroxy radicals reacting in the inlet, a significant background NO_2 signal – due to ambient NO_2 and to the reaction between O_3 and NO inside the inlet – is also observed. Consequently, the measurements in the inlet are modulated so that 1 min of amplification of the radical signal is alternated with 1 min of termination of the radical signal. The difference between the amplification and the termination mode signals consists in NO_2 formed only by HO_2 and RO_2 radicals. The PERCA deployed on the R/V *Brown* had two inlets (dual-channel), so that when one inlet was in amplification mode the other was in background mode, increasing the time resolution of the measurements to 1 min, compared to 2 min of a single-channel PERCA.

The total concentration of radicals is obtained by dividing the chain length by the measured concentration of NO_2 (Eq. 1). Since the concentration of OH is typically two orders of magnitude lower than the concentration of peroxy radicals, this is equivalent to the sum of HO_2 and organic peroxy radicals (RO_2).

$$([OH] + [HO_2] + [RO_2]) = \frac{\Delta NO_2}{CL} \tag{1}$$

The PERCA instrument deployed on the R/V *Brown* used one chemiluminescence detector (Scintrex LMA-3) per inlet to measure NO_2. The NO_2 detectors were calibrated every day using known concentrations of NO_2 from two permeation tubes located next to the inlets (Green et al., 2006).

Calibration of the Scintrex LMA-3 detectors was checked by comparison against a cavity ring-down (CRD) instrument (Osthoff et al., 2006), which gives an absolute measurement of NO_2. The two instruments were connected in series, so that NO_2 was first measured by the CRD and then by the Scintrex LMA-3. The result of the comparison is shown in Fig. 2. The Scintrex LMA-3 and the CRD agreed to within 9%, although the Scintrex LMA-3 overestimated NO_2 by 4.5 ppb (Fig. 2). The offset, however, did not affect the peroxy radical measurement, because they are determined

from the difference between the two NO_2 channels rather than from the absolute NO_2 concentration.

The largest uncertainty factor is the determination of the chain length (*CL*). During the R/V *Brown* cruise *CL* was determined approximately every 3–4 days via genera-
tion of a known concentration of CH_3O_2 radicals from the photolysis of methyl iodide (CH_3I) in zero air (Fleming et al., 2006). To validate this calibration method, *CL* was also determined using $CH_3C(O)O_2$ radicals. The calibration source of a Chemical Ionization Mass Spectrometer (CIMS, Slusher et al., 2004) used to measured PANs on the R/V *Brown* was put inside the PERCA inlet and heated to different temperatures to
inject different concentrations of acetyl peroxy radicals into the PERCA inlet. The chain lengths determined by the two procedures differed by less than 10%, a difference that may arise from the use of peroxy radicals with slightly different chain lengths, but that is well within the range of the estimated measurement error of the PERCA.

Previous work has shown the PERCA chain length to be dependent on both ambient
humidity and temperature (Salisbury et al., 2002; Reichert et al., 2003). Therefore, it is usually determined in dry air and then corrected using a calibration factor. However, the determination of *CL* during the experiment with the PAN source was carried out in ambient (humid) air. The agreement between the *CL* determined in ambient air with PAN and the *CL* determined in zero air with CH_3I demonstrates that the data collected
during the TexAQS 2006 cruise did not require a correction for relative humidity. This was also the case for a similar PERCA instrument during another field campaign under similarly high ambient humidity and temperature conditions (Andrés-Hernández et al., 2010). Raw data were only corrected for the RH dependence of the NO_2 measurements from the Scintrex LMA-3 detector using a correction factor ($\sim 30\%$) determined
in the laboratory after the campaign.

Combining the uncertainties in the measurement of NO_2 and in the determination of the *CL* and in the correction factor for the NO_2 detector, the total uncertainty of the instrument during the TexAQS 2006 cruise of the R/V *Brown* was 40% with a detection limit of 2 ppt.

A simple box-model (Sect. 4.1) was run for the clean conditions encountered in air masses from the remote regions of the Gulf of Mexico and the Atlantic Ocean. Under these conditions the chemical cycling is reasonably well understood (Sommariva et al., 2004) and the good agreement between the uncorrected $HO_2+\Sigma RO_2$ data and the box-model results supports the overall accuracy of the PERCA measurements.

2.2 Instruments on board the R/V *Brown*

A number of other measurements relevant to this work were deployed on the R/V *Brown* and are described in detail elsewhere (Parrish et al., 2009). NO and NO_2 were measured using a chemiluminescence technique (Ryerson et al., 2000), with a detection limit of 0.01 and 0.06 ppb, respectively. CO and O_3 by UV-fluorescence technique and the photolysis rates of several species were measured with filter radiometers (Stark et al., 2007). [222]Radon was detected using a dual flow loop two filter detector (Bates et al., 2008), located on the upper deck of the R/V *Brown*.

Speciated VOC (96 total) were measured by a dual channel gas chromatograph system with a flame ionization detector (GC-FID) on one channel and a mass spectrometer (GC-MS) on the other. The instrument, which collected 5 min samples every 25 min, measured the mixing ratios of C2-C9 VOC with a detection limit of 0.5–1 ppt depending on the species (Gilman et al., 2009). Acetaldehyde and acetic acid were measured by Proton Transfer Ion Trap Mass Spectrometry (PIT-MS, Warneke et al., 2005), while HCHO was measured by Tunable Infrared Laser Differential Absorption Spectroscopy (TILDAS, Herndon et al., 2007) with a detection limit of 75 ppt and a 7% accuracy.

NOAA's High Resolution Doppler Lidar (HRDL) performed measurements of atmospheric boundary layer wind, aerosol backscatter, and turbulence profiles with a resolution of 15 min and 30 m (Tucker et al., 2010). These measurements were used to estimate the mixing height, which determines the dilution of near surface emissions of pollutants by vertical mixing in the boundary layer.

The instruments, including the PERCA, were housed in sea containers mounted on one of the upper decks in the forward part of the R/V *Brown*, approximately 12 m above

the sea surface. The inlets were located at the top of a 8 m tower, approximately 20 m above the sea surface. The HRDL Lidar was located at the stern of the ship.

2.3 The TexAQS 2006 cruise of the R/V *Brown*

The Texas Air Quality Study 2006 campaign took place during the summer of 2006. The campaign was part of the more comprehensive TexAQS/GoMACCS (Gulf of Mexico Atmospheric Composition and Climate Study) regional air quality and climate change study and its main objective was to investigate air quality and meteorology along the Gulf coast of the United States and in particular around the Houston/Galveston area. The NOAA research vessel R/V *Brown* sailed from Charleston, South Carolina, on 27 July and arrived in Houston, Texas, on 2 August. Between 2 August and 11 September the R/V *Brown* cruised along the coast of Texas, inside Galveston Bay and up the Sabine River to Beaumont, Texas. The track of the ship is shown in Fig. 3, which also indicates several of the locations visited during the cruise. Approximately 20% of the entire research cruise was spent at a single location, Barbours Cut (Fig. 5), a commercial shipping dock south of the Houston Ship Channel and close to the site (LaPorte, Texas) of a previous field campaign (TexAQS 2000, Ryerson et al., 2003; Jobson et al., 2004).

The Houston/Galveston area is home to one of the busiest ports of the United States. The port opens at Galveston Bay and ends in the Houston Ship Channel (Fig. 5), which is currently one of the most important waterways for the movement of petrochemical products, goods and grains in North America. The Houston Ship Channel is approximately 160 m wide and 80 kilometers long and is entirely surrounded by loading docks and petrochemical industries. The ship traffic between the Houston Ship Channel and the Gulf of Mexico mostly consists of tankers, freighters and large number of barges and tugboats. This, together with the rest of the industrial activity and the urban traffic in and around the Greater Houston metropolitan area, results in high emissions of NO_x and VOC, responsible for the high photochemical activity and formation of ozone in the region (Ryerson et al., 2003; Parrish et al., 2009). The ocean along the coast of

Full Screen / Esc

Southern Texas is also subject to considerable ship traffic and a large number of oil extraction platforms, mostly located on the continental shelf. Other industrial areas are present all along the coast of Texas: during the 2006 cruise, the R/V *Brown* sampled in Port Arthur and in Beaumont, near the border with Louisiana, in Freeport and in Matagorda, southwest of Galveston along the Gulf Coast (Fig. 5).

The local meteorology in the Houston/Galveston region has a profound influence on ozone concentration and radical chemistry. Stagnant conditions over the shores of Galveston Bay can arise when moderate offshore synoptic-scale winds are strong enough to override and suppress the early afternoon bay breeze (Banta et al., 1998, 2005). This allows for accumulation of photochemical ozone over Galveston Bay, which is subsequently advected over Houston in the lowest few hundred meters by the late afternoon on-shore sea breeze. Tucker et al. (2010) also observed the effect of the synoptic conditions on boundary layer mixing height and impact on the concentration of ozone in this area.

Previous studies in the region (e.g. Ryerson et al., 2003; Jobson et al., 2004; Kleinman et al., 2005) have highlighted the special chemical characteristics of the Houston/Galveston area: co-located large emissions of NO$_x$ and of highly reactive VOC (particularly light alkenes) combined with the unique meteorology described above result in some of the highest concentrations of urban ozone in the U.S.. Measurements of peroxy radicals in such photochemically active air masses provide a unique look into their chemistry and assists in understanding the factors that influence ozone production across the region.

3   Measurements of HO$_2$+ΣRO$_2$

Total peroxy radicals were measured continuously (>90% of data coverage) from 28 July to 11 September on board the R/V *Brown* during TexAQS 2006. The entire dataset is shown in Fig. 3 and, together with measurements of O$_3$ photolysis rates (j(O^{1}D)), in Fig. 4. The concentrations of total peroxy radicals were clearly correlated with O$_3$

photolysis rates throughout the cruise; this is expected as ozone was always a major radical source, even in the most polluted areas, where HCHO and HONO were also important radical sources (Olaguer et al., 2009).

Day-time maximum mixing ratios of HO$_2$+ΣRO$_2$ ranged from 25 to 110 ppt. The highest levels were observed in the industrial areas, owing to the abundance of VOC, the precursors of peroxy radicals and of NO$_x$ (Fig. 1). During the first few days of the cruise (28 July to 2 August) the R/V *Brown* was en route from Charleston, South Carolina, to Houston, Texas (Fig. 5), sampling the cleanest air masses of the campaign. Measured day-time peroxy radicals were, on average, between 35 and 50 ppt during this period. Gilman et al. (2009) showed that VOC accounted for approximately 32% of the total OH reactivity and the most important VOC were formaldehyde (0.5 ppb), acetaldehyde (0.1 ppb) and light alkenes (0.01–0.06 ppb). CO and CH$_4$ accounted, respectively for 38% and 27% of the total OH reactivity (Gilman et al., 2009); it can be inferred that, during this period, HO$_2$+ΣRO$_2$ was comprised mostly of HO$_2$ and CH$_3$O$_2$. These measurements in clean marine air, originating in the subtropical Atlantic Ocean and the Caribbean region, can be considered representative of background marine conditions.

Peroxy radicals were also measured at night during the entire cruise with mixing ratios typically between 5 and 25 ppt, depending on the conditions and the location of the R/V *Brown*. On occasion, very high mixing ratios were measured, such as during the night of 7 September when the R/V *Brown* was docked in Jacinto Point at the entrance to the Houston Ship Channel (Fig. 5). On this night, HO$_2$+ΣRO$_2$ reached a campaign maximum of 134 ppt, which is likely related to night-time oxidation reaction (O$_3$ or NO$_3$) of highly reactive VOC. During the same evening, a plume composed of C2-C5 alkenes at a combined mixing ratio of 190 ppb was sampled (Gilman et al., 2009).

The measurements taken during the R/V *Brown* cruise were divided into 5 groups, defined by the location of the ship. They are referred to hereafter as: Ocean, Gulf Coast, Galveston Bay, Industrial Areas and Barbours Cut. Diurnal profiles of the

$HO_2 + \Sigma RO_2$ and NO_x measurements at each location are shown in Fig. 5. The data taken when the ship was in the Atlantic Ocean and in the Gulf of Mexico (Fig. 5) were divided between the Ocean and Gulf Coast groups using [222]Radon counts. [222]Radon is a by-product of the degradation of [238]Uranium with half-life of 3.82 days; it is commonly released in the atmosphere from granitic soils and rocks and therefore can be used as a tracer of continental influence. Gulf Coast air masses were rich in [222]Radon and contained continental outflow and anthropogenic influence, with higher mixing ratios of total peroxy radicals and NO_x (60 ppt and 0.7–1.2 ppb, respectively, Fig. 5). Ocean air masses poor in [222]Radon were less impacted by recent anthropogenic emissions and had lower mixing ratios of peroxy radicals and NO_x (30–35 ppt and 0.2–0.4 ppb, respectively, Fig. 5). The sources of peroxy radicals in these two areas were likewise different: in the Ocean they were formed mostly by CO and CH_4, which together accounted for about 65% of the total OH reactivity, on average. The role of VOC in the formation of peroxy radicals was mostly due to the reactivity of oxygenated compounds, especially formaldehyde and acetaldehyde (Gilman et al., 2009). In the Gulf Coast, owing to the outflow of polluted air from the continent, the production of peroxy radicals was controlled by VOC, particularly alkanes, alkenes and oxygenates, which accounted for a much larger fraction (∼53%, on average) of the reactivity of OH (Gilman et al., 2009).

The data grouped under Galveston Bay include all the measurements taken when the ship was in Galveston harbour and in Galveston Bay itself (Fig. 5). These data were affected especially by shipping emissions and, to a certain extent, by industrial emissions, but not as much as those grouped under Industrial Areas, which were taken close to the emission points (that is the Houston Ship Channel, Freeport, Matagorda and Beaumont, Fig. 3). Day-time peroxy radicals and NO_x mixing ratios were, on average, around 40–45 ppt and 20 ppb, respectively, in Galveston Bay, while they were about 45–50 ppt and 10 ppb, respectively, in the Industrial Areas (Fig. 5). Measurements in the Industrial Areas showed greater variability than those in other places (Fig. 5), partly because of the smaller number of samples in the diurnal averages of Fig. 5, and partly because of the spatial and temporal variability of local, industrial

Title Page

Abstract | Introduction

Conclusions | References

Tables | Figures

◄◄ | ►►

◄ | ►

Back | Close

Full Screen / Esc

Printer-friendly Version

Interactive Discussion

emission sources. The sources of peroxy radicals in these areas were dominated by oxidation of non-methane hydrocarbons, which accounted for 72% of the reactivity of OH (Gilman et al., 2009). While C2–C4 alkanes were the most abundant RO_2 precursors, the largest fraction of the OH reactivity was due to light alkenes and formaldehyde
5 (Gilman et al., 2009).

Although the chemical characteristics of the air masses sampled in Barbours Cut (Fig. 5, 5) were not dissimilar from those measured in the Galveston Bay or in the Industrial Areas (depending on the meteorology), these data were analyzed separately since this was the single location where the ship spent the most time; it is also ~ 6 km
10 from the ground site (LaPorte airport) of the TexAQS 2000 field campaign, thus enabling the most direct comparison of radical measurements between the two study years. Day-time mixing ratios of $HO_2+\Sigma RO_2$ in Barbours Cut were, on average, 30–35 ppt, with about 10–15 ppb of NO_x (Fig. 5). Air masses at this location were influenced principally by the neighbouring Houston Ship Channel and Texas City (Fig. 5)
15 and/or by air masses from Galveston Bay.

Barbours Cut measurements showed a distinctive decrease in $HO_2+\Sigma RO_2$ concentration around 12:00 GMT (07:00 local time), which was also observed, to a lesser extent, in the Industrial and Galveston Bay average diurnal profiles (Fig. 5). This dip in $HO_2+\Sigma RO_2$ was largely related to a corresponding increase in NO_x when emis-
20 sions from traffic and industries started to build up, just before sunrise, in the shallow (~ 200 m) nocturnal boundary layer (Tucker et al., 2010). The breakup of this shallow layer after sunrise and the subsequent mixing with cleaner air from aloft caused a sharp decrease in NO_x, CO and the precursor VOC and an increase in $HO_2+\Sigma RO_2$ concentrations.

25 Figure 6 shows the medians and the 10-th, 25-th, 75-th and 90-th percentiles of measured $HO_2+\Sigma RO_2$ concentrations plotted versus NO_x during the day in the different regions. As the ship moved from the Ocean to the Gulf Coast and into Galveston Bay (Fig. 6), there was a transition from low to high NO_x. Accordingly, the peroxy radical mixing ratios increased from 10–20 ppt in the clean marine boundary layer to several

tens of ppt in the most polluted areas.

The concentrations of $HO_2 + \Sigma RO_2$ peaked at intermediate $[NO_x]$ and decreased at higher $[NO_x]$, but the dependence of $HO_2 + \Sigma RO_2$ on nitrogen oxides is not always clear because of the high variability of the measurements in the polluted areas (like Barbours Cut and the Industrial Areas) compared to the clean Ocean. The concentrations of NO_x and the relationship with total peroxy radicals in Barbours Cut was similar to the Industrial Areas, although with lower $HO_2 + \Sigma RO_2$ concentrations (Fig. 5). Peroxy radicals mixing ratios in the Industrial Areas showed larger variability and were more influenced by outliers, probably because of individual emission plumes characterized by high levels of reactive VOC and NO_x from nearby industrial complexes (the PERCA measurements frequency was 1 min, sufficient to detect individual plumes). By contrast, peroxy radicals in Barbours Cut, which were farther from localized emissions and underwent more mixing and chemistry with the regional background air, were somewhat less variable.

4 Photochemical formation of O_3

4.1 Net photochemical ozone formation

Total peroxy radical measurements have been used in several previous studies (e.g., Salisbury et al., 2002; Fleming et al., 2006; Parker et al., 2009) to calculate the net photochemical ozone formation (*Net(*O_3*)*). *Net(*O_3*)* is defined as the difference between in-situ photochemical production and loss of ozone (Eq. 2). The production of ozone is equivalent to the formation rate of NO_2, whose photolysis is the only known mechanism for ozone formation in the troposphere (Reaction R2), via the reaction of HO_2 and organic peroxy radicals with NO (Eq. 3). The loss of ozone is equal to its photolysis rate times the fraction (f, Eq. 5) of the $O(^1D)$ product that goes on to react with water vapor rather than quenching to produce atomic oxygen and, ultimately, reform ozone. Ozone is also lost via reactions with OH and HO_2 (Eq. 4). The

reaction of ozone with NO forms NO_2 which reforms O_3, so it is neutral in terms of the ozone budget and not included in Eq. (4). The rate coefficient used for RO_2+NO was $2.54 \times 10^{-12} * \exp(360/T) \, cm^3 molecule^{-1} s^{-1}$, which is the generic value used in the Master Chemical Mechanism (MCM, http://mcm.leeds.ac.uk/) for all RO_2+NO reactions for which no experimental values are available. The other rate coefficients were taken from the 2007 IUPAC evaluation (Atkinson et al., 2006).

$$Net(O_3) = Prod(O_3) - Loss(O_3) \tag{2}$$

$$Prod(O_3) = (k_{HO_2+NO} * [HO_2] + k_{RO_2+NO} * [RO_2]) * [NO] \tag{3}$$

$$Loss(O_3) = (f * j(O^1D) + k_{OH+O_3} * [OH] + k_{HO_2+O_3} * [HO_2]) * [O_3] \tag{4}$$

$$f = \frac{k_{O^1D+H_2O} * [H_2O]}{k_{O^1D+H_2O} * [H_2O] + k_{O^1D+M} * [M]} \tag{5}$$

Measurements of NO, O_3, $j(O^1D)$ and H_2O were used in Eqs. (3), (4), (5). The concentration of inorganic (HO_2) and total organic (RO_2) in Eqs. (3), (4) were calculated using measured $HO_2+\Sigma RO_2$ and an $HO_2/(HO_2+\Sigma RO_2)$ ratio calculated with a box-model based upon the MCM. The concentration of OH in Eq. (4) was also calculated with the box-model. The model contained the oxidation scheme of 65 measured VOC, plus a complete inorganic mechanism taken from the IUPAC evaluation and was constrained to the chemical and physical parameters measured on board the R/V *Brown* during the cruise. The model setup and assumptions have been described in detail in previous publications (Sommariva et al., 2006, 2009).

A local sensitivity analysis was performed on the calculated *Prod(O₃)*, *Loss(O₃)* and *Net(O₃)* to assess the relative importance of each parameter and of the assumptions made. The local sensitivity analysis was made by varying the value of the input parameters in Eqs. (2), (3) and (4) (i.e., NO, O_3, $HO_2+\Sigma RO_2$, k_{HO_2+NO}, k_{RO_2+NO}, $k_{HO_2+O_3}$, $j(O^1D)$, $HO_2/(HO_2+\Sigma RO_2)$ and OH) by ±1%. The percent variation in the calculated

Full Screen / Esc

Printer-friendly Version

Interactive Discussion

$Prod(O_3)$, $Loss(O_3)$ and $Net(O_3)$ is indicated as $\Delta X^{\pm 1\%}$ and used to calculate the sensitivity index (SI, Eq. 6) for each of these parameters.

$$SI = \frac{\%\Delta X^{+1\%} - \%\Delta X^{-1\%}}{100 \times 0.02} \qquad (6)$$

The results of the local sensitivity analysis are shown in Table 1 as campaign averages of the calculated SI. Photochemical production and loss of O_3 were not very sensitive to the calculated concentration of OH or to the calculated $HO_2/(HO_2+\Sigma RO_2)$ ratio, but they were sensitive to the concentrations of NO, O_3 and $HO_2+\Sigma RO_2$, which were measured in-situ. The net photochemical ozone formation was most sensitive to NO and $HO_2+\Sigma RO_2$, whose overall uncertainty was about 4% (Sect. 2.2) and 40% (Sect. 2.1), respectively. Therefore $HO_2+\Sigma RO_2$ was the most critical parameter in determining $Net(O_3)$. If the measured concentration of $HO_2+\Sigma RO_2$ was changed by ±40%, calculated $Net(O_3)$ changed, on average, by ±39–41% (Eq. 2).

The net photochemical ozone formation was also sensitive to k_{RO_2+NO} (Table 1), a generic rate coefficient for the reaction of organic peroxy radicals with NO. The composition of the peroxy radical pool was unknown; therefore, all organic peroxy radicals had to be considered as a single species for the purpose of this calculation. In principle, an MCM model could yield this information; however experimental kinetic data are not available for every individual species in the MCM, so a generic rate coefficient would have to be used regardless. The error in this assumption is difficult to estimate, but, considering the typical uncertainty range of known reactions involving peroxy radicals (15–60%), it is probably comparable to the uncertainty in the $HO_2+\Sigma RO_2$ measurements (Sect. 2.1).

4.2 Ozone formation during the R/V *Brown* cruise

The net photochemical formation, $Net(O_3)$, calculated with Eq. (2) during daylight hours was divided on the basis of the location of the R/V *Brown*, in the same way as the

Title Page

Abstract | Introduction

Conclusions | References

Tables | Figures

|◄ | ►|

◄ | ►

Back | Close

Full Screen / Esc

HO$_2$+ΣRO$_2$ data (Sect. 3). The median diurnal profiles of *Prod(*O$_3$*)* and *Loss(*O$_3$*)* in each location are shown in Fig. 7. Photochemical production (Eq. 3) was 1–2 orders of magnitude higher than photochemical loss (Eq. 4) in all areas, except in the Ocean, where the two components of Eq. (2) had similar magnitude, resulting sometimes in

5 net photochemical ozone destruction (negative *Net(*O$_3$*)*). *Loss(*O$_3$*)* was similar in all locations, because the main component in Eq. (4) was the photolysis of ozone, which accounted typically for 70–95% of *Loss(*O$_3$*)*. This also explains the characteristic diurnal variation of photochemical ozone loss in Fig. 7.

The lowest median values of *Prod(*O$_3$*)* were observed in the Ocean and along the

10 Gulf Coast (0.6–12 ppb/h), while the highest median values of *Prod(*O$_3$*)* were observed in Galveston Bay and Industrial Areas (up to 100 ppb/h). *Prod(*O$_3$*)* did not show a clear diurnal cycle in any of the sampled locations (Fig. 7), although it tended to decrease in the afternoon in the Gulf Coast, Barbours Cut and in the Industrial Areas probably due to the decrease in the HO$_2$+ΣRO$_2$ concentrations. In the Ocean and Galveston Bay,

15 photochemical formation of ozone was sustained in the late afternoon, by oxygenated VOC, which photolyze at longer wavelengths and act as radical precursors in these areas (Sect. 3).

The high values of *Prod(*O$_3$*)* shown in Fig. 7 resulted in high values of net photochemical ozone production, particularly in Barbours Cut, Galveston Bay and in the In-

20 dustrial Areas. The high production rates were comparable to those observed and calculated at the LaPorte site during the previous TexAQS 2000 campaign (see Sect. 4.3) and were mostly driven by high concentrations of NO (Eq. 3). In Barbours Cut and in the Industrial Areas, the median mixing ratios of NO were 7.4 ppb and 13 ppb, respectively, which led to production rates on the order of tens to hundreds of ppb/h. While

25 high, these values are not uncommon. Kleinman et al. (2005) reported ozone production rates on the order of tens of ppb/h in several U.S. urban areas and, in particular, in Houston, Texas, where production rates were up to 155 ppb/h. The higher ozone production rates in Houston compared to other urban areas were attributed to the co-location of NO$_x$ and highly reactive olefins emissions from the petrochemical plants in

Title Page

Abstract	Introduction
Conclusions	References
Tables	Figures

◄ | ►

◄ | ►

Back | Close

Full Screen / Esc

Printer-friendly Version

Interactive Discussion

the Houston/Galveston area. Kleinman et al. (2005) also noted, by looking at data from Philadelphia, Pennsylvania, and Phoenix, Arizona, that morning and afternoon ozone production rates were generally comparable. Although a straightforward comparison is not possible, this is consistent with the data presented in this work (Fig. 7).

5   The occurrence of a large number of high *Prod(*O$_3$*)* episodes was likely related to sampling of individual plumes characterized by high concentrations of NO$_x$ and reactive VOC, especially in the Industrial Areas. This tends to bias the analysis of the measurements towards higher values. To better understand the probability of such events, the net photochemical ozone formation (*Net(*O$_3$*)*, Eq. 2) at different locations
10 of the R/V *Brown* cruise is shown in Fig. 8 as frequency distributions. Except in the Ocean, *Net(*O$_3$*)* was positive, indicating that these were all ozone producing areas. In the Ocean, ozone destroying conditions were often encountered, when very clean air masses from the central Gulf of Mexico or from the Atlantic Ocean were sampled (Fig. 8). The median *Net(*O$_3$*)* was 0.5 ppb/h in Ocean, although the average value
15 was higher (5.5 ppb/h). In the Gulf Coast, the median *Net(*O$_3$*)* was 2.4 ppb/h (and the average 7.4 ppb/h). These values are comparable to the net ozone formation rates reported by previous studies in the semi-polluted and clean marine boundary layer (e.g., Salisbury et al., 2002; Fleming et al., 2006).

The median *Net(*O$_3$*)* was much lower than the average *Net(*O$_3$*)* be-
20 cause of the presence of a large number of outliers (Fig. 8). This was related to the high variability in the local emissions, particularly in the Industrial Areas, where a clear distribution of the *Net(*O$_3$*)* values was not evident. It implies that the measurements taken in the Industrial Areas were a collection of individual plumes from different industrial sources rather than representative of the area as a whole. This is also true
25 for Galveston Bay data, which were likely influenced by emissions from passing ships, tugboats and barges. *Net(*O$_3$*)* was very high in the Industrial Areas, Barbours Cut and Galveston Bay with values in the range of tens up to hundreds of ppb/h. The median *Net(*O$_3$*)* in the Industrial Areas was 43.8 ppb/h, although values as high as several hundreds of ppb/h were as frequent as lower values (Fig. 8). In Barbours Cut and

Galveston Bay the median *Net(*O$_3$*)* was similar, between 23 and 26 ppb/h, but the average was lower in Barbours Cut (60 vs. 150 ppb/h), because of the lower HO$_2$+ΣRO$_2$ concentrations measured in this location (Sect. 3). Ozone formation in Barbours Cut is discussed in more detail in Sect. 4.3 in relation to VOC reactivity and the geographical distribution of the emission sources around the commercial shipping dock (Fig. 5).

Sustained photochemical ozone formation rates on the order of tens or even hundreds of ppb/h would rapidly generate extremely high concentrations of ozone, much larger than observed by, for example, the ozone monitoring network around the Houston area. Kleinman et al. (2005) noted that while high ozone events were preceded by periods of high *Prod(*O$_3$*)*, not all periods of high *Prod(*O$_3$*)* necessarily led to high ozone events. This is because dilution also plays an important role in determining the downwind concentration of ozone and can be more important than the photochemical processes (Banta et al., 2005; Tucker et al., 2010). For example, during TexAQS 2006, Langford et al. (2009) found that high photochemical activity on 4 August resulted in comparatively low ozone concentrations because of the strong winds that lowered the regional ozone background.

4.3 Ozone formation in Barbours Cut

In Barbours Cut (Fig. 3), the R/V *Brown* was either docked or stationary and therefore it is possible to analyze the net photochemical O$_3$ formation on the basis of the local wind direction and relate *Net(*O$_3$*)* to the sources around the shipping dock. Figure 9 shows *Net(*O$_3$*)* and local wind direction polar distributions for Barbours Cut together with the OH reactivity of different classes of VOC (measured in s^{-1} as 1/τ_{OH}, where τ_{OH} is the lifetime of a VOC with respect to reaction with OH). The S-SW and S-SE sectors were the most frequently sampled during the period when the R/V *Brown* was in Barbours Cut, while only occasionally air masses coming from N and NW sectors were sampled.

The highest values of *Net(*O_3*)* were measured when the wind was from the E–SE and E–NE sector (Fig. 9). Given the location of Barbours Cut (Fig. 5), these correspond to air masses that had spent some time over Galveston Bay. As explained earlier (Sect. 2.3) and discussed in previous work (Banta et al., 1998, 2005), the particular meteorology of the area can lead to stagnant conditions around the northern shore of Galveston Bay, leading to a buildup of ozone concentrations that are then transported back over Houston by the onshore sea breeze.

The OH reactivities of different VOC classes can be used to investigate which species most influenced O_3 formation in different sectors. Alkenes clearly were the dominant class of reacting VOC, with values of $1/\tau_{OH}$ on the order of tens of sec^{-1} (Fig. 9), followed by alkanes, biogenics, oxygenates and monomers (e.g., 1,3-butadiene and vinyl acetate), with values of $1/\tau_{OH}$ on the order of a few s^{-1}. Aromatics, halogenated VOC and nitrogen or sulphur containing VOC (such as DMS) showed the lowest reactivity to OH (Fig. 9). This is consistent with the analysis of Gilman et al. (2009), who showed that the concentration of OH was controlled by alkenes, C2–C4 alkanes and highly reactive species, such as isoprene, oxygenates, 1,3-butadiene and vinyl acetate.

The importance of the different classes in each sector was varied and was dependent on the emission sources surrounding Barbours Cut. Alkanes, alkenes and momomers showed a similar pattern, which can be traced to common emissions of industrial origin. These species were most important in air masses from the E-NE and W-SW sectors (Fig. 9), corresponding to industries on either side of the Houston Ship Channel (Fig. 5). Aromatics, although much less reactive, contributed to the OH reactivity in these air masses and also in air masses from the S–SW sector (Fig. 9). The different pattern of aromatics is related to the fact that these species are of urban (i.e., traffic) as well as industrial origin and therefore impacted a broader range of air masses. In the SW, S and SE sectors, OH reactivity was largely controlled by biogenic and oxygenated VOC. The S–SW sector, in particular, was dominated by biogenics (mostly isoprene) and their oxygenated products, such as methyl vinyl ketone and methacrolein (Gilman

Title Page

Abstract | Introduction

Conclusions | References

Tables | Figures

◄ | ►►

◄ | ►

Back | Close

Full Screen / Esc

Printer-friendly Version

Interactive Discussion

et al., 2009). The E–SE sector was almost completely dominated by oxygenated VOC (Fig. 9), the most important of which was formaldehyde. The main source of HCHO was determined to be secondary formation from the oxidation of hydrocarbons rather than primary emission (Gilman et al., 2009). As explained earlier, these air masses were recirculated from Galveston Bay and contained more processed air.

To summarize, the highest net ozone formation rates were measured in the E-SE sector and the most important precursors were oxygenated VOC and, to a lesser extent, biogenic VOC (Fig. 9). In the E–NE and in the W–SW sectors, on the other hand, the most important ozone precursors were alkenes, followed by alkanes and monomers (Fig. 9). Biogenics, followed by oxygenates, were the most important precursors in the S–SW sector (Fig. 9). Other species, such as aromatics and halogenated VOC, contributed very little to reactivity of OH and hence to the formation of ozone, either because of lower emissions or because of slower oxidation rates.

The measurements taken in Barbours Cut can be compared with those taken at LaPorte airport during the previous TexAQS 2000 campaign. LaPorte is only 6 km west of Barbours Cut (Fig. 5). In 2000, HO_2 was measured by laser-induced fluorescence, but there were no measurements of organic peroxy radicals. Therefore, a direct comparison between the measurements in 2000 and in 2006 is not possible. However, a box-model (Frost et al., 1999) can be used as a proxy to compare the results; the box-model was constrained to the measurements taken in 2000 at LaPorte.

In Fig. 10, modelled HO_2 and $HO_2+\Sigma RO_2$ were compared to measured HO_2 and $2 \times HO_2$, respectively, for the 2000 campaign at LaPorte; $2 \times HO_2$ was used as an estimate of total peroxy radicals, a reasonable assumption in urban influenced outflow (Wood et al., 2009). The agreement between the model and the measurements during TexAQS 2000 was very good: the concentrations were comparable to the $HO_2+\Sigma RO_2$ measurements taken at Barbours Cut in 2006 and showed similar dependence on $[NO_x]$ (Fig. 10).

In-situ O_3 photochemical production (*Prod(O_3)*, Eq. 3) was calculated using only HO_2 for the 2000 campaign: there was good agreement between the modelled and

the measured $Prod(O_3)$ and a clear dependence on NO_x mixing ratio, with a peak in $Prod(O_3)$ around 30–40 ppb of NO_x. $Prod(O_3)$ calculated using $HO_2+\Sigma RO_2$ from the TexAQS 2000 model was then compared with the one calculated from the $HO_2+\Sigma RO_2$ measurements in TexAQS 2006 in Fig. 10. Despite the difference in space and time

5 between the two datasets, there is remarkable agreement and the NO_x dependence of $Prod(O_3)$ was similar in 2000 and 2006. The measurements made in 2006 also showed increasing $Prod(O_3)$ with $[NO_x]$, with a maximum centered around 30–40 ppb (Fig. 10). The comparisons in Fig. 10 suggests that conditions in LaPorte in 2000 and in Barbours Cut in 2006 were very similar. The level of $[NO_x]$ was somewhat lower in

10 2006, consistent with other observations (Parrish et al., 2009) and ozone production remained NO_x-limited in this area, likely because of the abundance of VOC emitted from the surrounding industries.

5   Summary and conclusions

Measurements of total peroxy radicals ($HO_2+\Sigma RO_2$) were made during the TexAQS

15 2006 cruise of the R/V *Brown* with a dual-channel PEroxy Radical Chemical Amplifier (PERCA). The ship sailed across the Gulf of Mexico and along the Gulf coast of Texas, spending most of the time in the highly industrialized Houston/Galveston region.

Mixing Ratios of $HO_2+\Sigma RO_2$ ranged from 25 to 110 ppt during the day and from 5 to 25 ppt (with a a maximum of 134 ppt) during the night. The data were divided according

20 to the location of the R/V *Brown* into five areas – Ocean, Gulf Coast, Galveston Bay, Industrial Areas and Barbours Cut (Fig. 3) – and analyzed in conjunction with measure-ments of nitrogen oxides, VOC, photolysis rates and [222]Radon, in order to assess the differences between the 5 regions in terms of radical sources and sinks. The lowest $HO_2+\Sigma RO_2$ mixing ratios (30–35 ppt) were observed in the Ocean and were mostly

25 related to the reactivity of CO, CH_4 and oxygenated VOC. The highest $HO_2+\Sigma RO_2$ mixing ratios (45–50 ppt) were observed in the Industrial Areas and were related to highly reactive VOC (e.g., alkenes, isoprene, butadiene).

Title Page

Abstract | Introduction

Conclusions | References

Tables | Figures

◄ | ►►

◄ | ►

Back | Close

Full Screen / Esc

Printer-friendly Version

Interactive Discussion

The measurements of total peroxy radicals were used to calculate instantaneous in-situ photochemical production (*Prod(*O$_3$*)*) and loss (*Loss(*O$_3$*)*) rates of ozone and the net photochemical ozone formation (*Net(*O$_3$*) = Prod(*O$_3$*)-Loss(*O$_3$*)*). The median net photochemical ozone formation rates ranged from 0.5 ppb/h in the Ocean to 44 ppb/h in the Industrial Areas, which is consistent with previous studies. Ozone destroying conditions (*Net(*O$_3$*) < 0* ppb/h) were also found in very clean air masses from the open Atlantic Ocean or Gulf of Mexico. Net photochemical ozone formation rates in the Industrial Areas were heavily affected by individual plumes, rich in highly reactive VOC from petrochemical industries, leading to *Net(*O$_3$*)* values of several tens of ppb/h. Such high ozone formation rates are characteristic of near-source regions and are limited in both time and space (e.g., related to single intermittent plumes).

The net photochemical ozone formation rates determined in Barbours Cut, south of the Houston Ship Channel, were analyzed in relation to local wind direction and VOC reactivity. The highest *Net(*O$_3$*)* were measured in air masses from the E-SE sector (i.e., from the Bay of Galveston) and were related mostly to oxygenated and biogenic VOC. Air masses from the E-NE and the W-SW sectors (i.e., from the Industrial Areas) were mostly related to alkenes, alkanes and monomers (e.g., 1,3-butadiene and vinyl acetate).

Finally, the results obtained during TexAQS 2006 were qualitatively compared to the results obtained during the previous TexAQS 2000 campaign, when HO$_2$ measurements were made at a nearby location (LaPorte airport, south of Houston and 6 km from Barbours Cut). The two datasets agreed reasonably well and showed a similar dependence on nitrogen oxides, indicating that ozone formation in the Houston area were NO$_x$-limited due to strong emissions of reactive VOC.

Title Page

Abstract | Introduction

Conclusions | References

Tables | Figures

|◄ | ►|

◄ | ►

Back | Close

Full Screen / Esc

Printer-friendly Version

Interactive Discussion

References

Andrés-Hernández, M. D., Stone, D., Brookes, D. M., Commane, R., Reeves, C. E., Huntrieser, H., Heard, D. E., Monks, P. S., Burrows, J. P., Schlager, H., Kartal, D., Evans, M. J., Floquet, C. F. A., Ingham, T., Methven, J., and Parker, A. E.: Peroxy radical partitioning during the AMMA radical intercomparison exercise, Atmos. Chem. Phys. Discuss., 10, 8447–8486, doi:10.5194/acpd-10-8447-2010, 2010. 23115

Atkinson, R., Cox, R. A., Crowley, J. N., Hampson, R. F., Hynes, R. G., Jenkin, M. E., Kerr, J. A., Rossi, M. J., and Troe, J.: Summary of evaluated kinetic and photochemical data for atmospheric chemistry, Tech. rep., IUPAC Subcommittee on Gas Kinetic Data Evaluation for Atmospheric Chemistry, http://www.iupac-kinetic.ch.cam.ac.uk/, 2006. 23123

Banta, R. M., Senff, C. J., White, A. B., Trainer, M., McNider, R. T., Valente, R. J., Mayor, S. D., Alvarez, R. J., Hardesty, R. M., Parrish, D., and Fehsenfeld, F. C.: Daytime buildup and nighttime transport of urban ozone in the boundary layer during a stagnation episode, J. Geophys. Res., 103, 22519–22544, 1998. 23118, 23128

Banta, R. M., Senff, C. J., Nielsen-Gammon, J., Darby, L. S., Ryerson, T. B., Alvarez, R. J., Sandberg, S. P., Williams, E. J., and Trainer, M.: A bad air day in Houston, B. Am. Meteorol. Soc., 86, 657–669, 2005. 23118, 23127, 23128

Bates, T. S., Quinn, P. K., Coffman, D., Schulz, K., Covert, D. S., Johnson, J. E., Williams, E. J., Lerner, B. M., Angevine, W. M., Tucker, S. C., Brewer, W. A., and Stohl, A.: Boundary layer aerosol chemistry during TexAQS/GoMACCS 2006; insights into aerosol sources and transformation processes, J. Geophys. Res., 113, D00F01, doi:10.1029/2008JD010023, 2008. 23116

Cantrell, C. A., Stedman, D. H., and Wendel, G. J.: Measurement of atmospheric peroxy radicals by chemical amplification, Anal. Chem., 56, 1496–1502, 1984. 23113

Cantrell, C. A., Shetter, R. E., Gilpin, T. M., and Calvert, J. G.: Peroxy radicals measured during Mauna Loa Observatory Photochemistry Experiment 2: the data and first analysis, J. Geophys. Res., 101, 14643–14652, 1996. 23113

Fleming, Z. L., Monks, P. S., Rickard, A. R., Heard, D. E., Bloss, W. J., Seakins, P. W., Still, T. J., Sommariva, R., Pilling, M. J., Morgan, R., Green, T. J., Brough, N., Mills, G. P., Penkett, S. A., Lewis, A. C., Lee, J. D., Saiz-Lopez, A., and Plane, J. M. C.: Peroxy radical chemistry and the control of ozone photochemistry at Mace Head, Ireland during the summer of 2002, Atmos. Chem. Phys., 6, 2193–2214, doi:10.5194/acp-6-2193-2006, 2006. 23113, 23115,

RO$_2$ measurements and O$_3$ production during TexAQS 2006

R. Sommariva et al.

Title Page

Abstract	Introduction
Conclusions	References
Tables	Figures

◄◄ ►►

◄ ►

Back Close

Full Screen / Esc

Printer-friendly Version

Interactive Discussion

23122, 23126

Frost, G. J., Trainer, M., Mauldin, R. L., Eisele, F. L., Prevot, A. S. H., Flocke, S. J., Madronich, S., Kok, G., Schillawski, R. D., Baumgarden, D., and Bradshaw, J.: Photochemical modeling of OH level during the First Areosol Characterization Experiment (ACE1), J. Geophys. Res., 104, 16041–16052, 1999. 23129

Gilman, J. B., Kuster, W. C., Goldan, P. D., Herndon, S. C., Zahniser, M. S., Tucker, S. C., Brewer, W. A., Lerner, B. M., Williams, E. J., Harley, R. A., Fehsenfeld, F. C., Warneke, C., and de Gouw, J. A.: Measurements of volatile organic compounds during the 2006 TexAQS/GoMACCS campaign: industrial influences, regional characteristics, and diurnal dependencies of the OH reactivity, J. Geophys. Res., 114, D00F06, doi: 10.1029/2008JD011525, 2009. 23116, 23119, 23120, 23121, 23128, 23129

Green, T. J., Reeves, C. E., Fleming, Z. L., Brough, N., Rickard, A. R., Bandy, B. J., Monks, P. S., and Penkett, S. A.: An improved dual channel PERCA instrument for atmospheric measurements of peroxy radicals, J. Environ. Monitor., 8, 530–536, 2006. 23113, 23114

Herndon, S. C., Zahniser, M. S., Nelson, D. D., Shorter, J., McManus, J. B., Jiménez, R., Warneke, C., and de Gouw, J. A.: Airborne measurements of HCHO and HCOOH during the New England Air Quality Study 2004 using a pulsed quantum cascade laser spectrometer, J. Geophys. Res., 112, D10S03, doi:10.1029/2006JD007600, 2007. 23116

Jobson, B. T., Berkowitz, C. M., Kuster, W. C., Goldan, P. D., Williams, E. J., Fehsenfeld, F. C., Apel, E. C., Karl, T., Lonneman, W. A., and Riemer, D.: Hydrocarbon source signatures in Houston, Texas: influence of the petrochemical industry, J. Geophys. Res., 109, D24305, doi:10.1029/2004JD004887, 2004. 23117, 23118

Kleinman, L. I., Daum, P. H., Lee, Y., Nunnermacker, L. J., Springston, S. R., Weinstein-Lloyd, J., and Rudolph, J.: A comparative study of ozone production in five U.S. metropolitan areas, J. Geophys. Res., 110, D02301, doi:10.1029/2004JD005096, 2005. 23118, 23125, 23126, 23127

Langford, A. O., Senff, C. J., Banta, R. M., Hardesty, R. M., Alvarez, R. J., Sandberg, S. P., and Darby, L. S.: Regional and local background ozone in Houston during the Texas Air Quality Study 2006, J. Geophys. Res., 114, D00F12, doi:10.1029/2008JD011687, 2009. 23127

Monks, P. S.: Gas-phase radical chemistry in the troposphere, Chem. Soc. Rev., 34, 376–395, 2005. 23112

Monks, P. S., Carpenter, L. J., Penkett, S. A., Ayers, G. P., Gillett, R. W., Galbally, I. E., and Meyer, C. P.: Fundamental ozone photochemistry in the remote marine boundary layer: the

SOAPEX experiment, measurement and theory, Atmos. Environ., 32, 3647–3664, 1998. 23113

Olaguer, E. P., Rappenglück, B., Lefer, B., Stutz, J., Dibb, J., Griffin, R., Brune, W. H., Shauck, M., Buhr, M., Jeffries, H., Vizuete, W., and Pinto, J. P.: Deciphering the role of radical precursors during the Second Texas Air Quality Study, J. Air Waste Manag. Assoc., 59, 1258–1277, 2009. 23119

Osthoff, H. D., Sommariva, R., Baynard, T., Pettersson, A., Williams, E. J., Lerner, B. M., Roberts, J. M., Stark, H., Goldan, P. D., Kuster, W. C., Bates, T. S., Coffman, D., Ravishankara, A. R., and Brown, S. S.: Observation of daytime N_2O_5 in the marine boundary layer during New England Air Quality Study-Intercontinental Transport and Chemical Transformation 2004, J. Geophys. Res., 111, D23S14, doi:10.1029/2006JD007593, 2006. 23114

Parker, A. E., Monks, P. S., Wyche, K. P., Balzani-Lv, J. M., Staehelin, J., Reimann, S., Legreid, G., Vollmer, M. K., and Steinbacher, M.: Peroxy radicals in the summer free troposphere: seasonality and potential for heterogeneous loss, Atmos. Chem. Phys., 9, 1989–2006, doi:10.5194/acp-9-1989-2009, 2009. 23113, 23122

Parrish, D. D., Allen, D. T., Bates, T. S., Estes, M., Fehsenfeld, F. C., Feingold, G., Ferrare, R., Hardesty, R. M., Meagher, J. F., Nielsen-Gammon, J. W., Pierce, R. B., Ryerson, T. B., Seinfeld, J. H., and Williams, E. J.: Overview of the Second Texas Air Quality Study (TexAQS II) and the Gulf of Mexico Atmospheric Composition and Climate Study (GoMACCS), J. Geophys. Res., 114, D00F13, doi:10.1029/2009JD011842, 2009. 23112, 23116, 23117, 23130

Reichert, L., Andrés-Hernández, M. D., Stöbener, D., Burkert, J., and Burrows, J. P.: Investigation of the effect of water complexes in the determination of peroxy radical ambient concentrations: implications for the atmosphere, J. Geophys. Res., 108, 4017, doi: 10.1029/2002JD002152, 2003. 23115

Ryerson, T. B., Williams, E. J., and Fehsenfeld, F. C.: An efficient photolysis system for fast-response NO_2 measurements, J. Geophys. Res., 105, 26447–26461, 2000. 23116

Ryerson, T. B., Trainer, M., Angevine, W. M., Brock, C. A., Dissly, R. W., Fehsenfeld, F. C., Frost, G. J., Goldan, P. D., Holloway, J. S., Hübler, G., Jakoubek, R. O., Kuster, W. C., Neuman, J. A., Nicks, D. K., Parrish, D. D., Roberts, J. M., Sueper, D. T., Atlas, E. L., Donnelly, S. G., Flocke, F., Fried, A., Potter, W. T., Schauffler, S., Stroud, V., Weinheimer, A. J., Wert, B. P., Wiedinmyer, C., Alvarez, R. J., Banta, R. M., Darby, L. S., and Senff, C. J.: Effect of petrochemical industrial emissions of reactive alkenes and NO_x on tropospheric ozone formation

Title Page

Abstract | Introduction

Conclusions | References

Tables | Figures

|◄ | ►|

◄ | ►

Back | Close

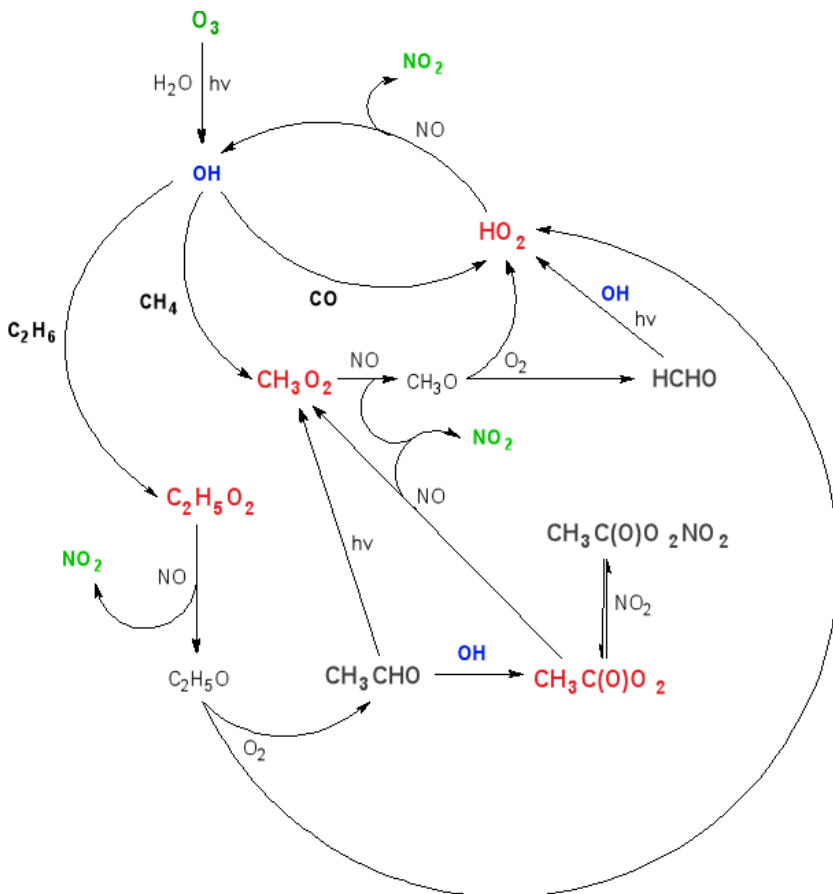Full Screen / Esc

Printer-friendly Version

Interactive Discussion

in Houston, Texas, J. Geophys. Res., 108, 4249, doi:10.1029/2002JD003070, 2003. 23117, 23118

Salisbury, G., Monks, P. S., Bauguitte, S., Bandy, B. J., and Penkett, S. A.: A seasonal comparison of the ozone photochemistry in clean and polluted air masses at Mace Head, Ireland, J.
5   Atmos. Chem., 41, 163–187, 2002. 23113, 23115, 23122, 23126

Slusher, D. L., Huey, L. G., Tanner, D. J., Flocke, F. M., and Roberts, J. M.: A thermal dissociation-chemical ionization mass spectrometry (TD-CIMS) technique for the simultaneous measurement of peroxyacyl nitrates and dinitrogen pentoxide, J. Geophys. Res., 109, D19315, doi:10.1029/2004JD004670, 2004. 23115

10   Sommariva, R., Haggerstone, A.-L., Carpenter, L. J., Carslaw, N., Creasey, D. J., Heard, D. E., Lee, J. D., Lewis, A. C., Pilling, M. J., and Zádor, J.: OH and HO_2 chemistry in clean marine air during SOAPEX-2, Atmos. Chem. Phys., 4, 839–856, doi:10.5194/acp-4-839-2004, 2004. 23116

Sommariva, R., Bloss, W. J., Brough, N., Carslaw, N., Flynn, M., Haggerstone, A.-L., Heard,
15   D. E., Hopkins, J. R., Lee, J. D., Lewis, A. C., McFiggans, G., Monks, P. S., Penkett, S. A., Pilling, M. J., Plane, J. M. C., Read, K. A., Saiz-Lopez, A., Rickard, A. R., and Williams, P. I.: OH and HO_2 chemistry during NAMBLEX: roles of oxygenates, halogen oxides and heterogeneous uptake, Atmos. Chem. Phys., 6, 1135–1153, doi:10.5194/acp-6-1135-2006, 2006. 23123

20   Sommariva, R., Osthoff, H. D., Brown, S. S., Bates, T. S., Baynard, T., Coffman, D., de Gouw, J. A., Goldan, P. D., Kuster, W. C., Lerner, B. M., Stark, H., Warneke, C., Williams, E. J., Fehsenfeld, F. C., Ravishankara, A. R., and Trainer, M.: Radicals in the marine boundary layer during NEAQS 2004: a model study of day-time and night-time sources and sinks, Atmos. Chem. Phys., 9, 3075–3093, doi:10.5194/acp-9-3075-2009, 2009. 23123

25   Stark, H., Lerner, B. M., Schmitt, R., Jakoubek, R., Williams, E. J., Ryerson, T. B., Sueper, D. T., Parrish, D. D., and Fehsenfeld, F. C.: Atmospheric in situ measurement of nitrate radical (NO_3) and other photolysis rates using spectroradiometry and filter radiometry, J. Geophys. Res., 112, D10S04, doi:10.1029/2006JD007578, 2007. 23116

Tucker, S. C., Banta, R. M., Langford, A. O., Senff, C. J., Brewer, W. A., Williams, E. J., Lerner,
30   B. M., Osthoff, H., and Hardesty, R. M.: Relationships of coastal nocturnal boundary layer winds and turbulence to Houston ozone concentrations during TexAQS 2006, J. Geophys. Res., 115, D10304, doi:10.1029/2009JD013169, 2010. 23116, 23118, 23121, 23127

Warneke, C., Kato, S., de Gouw, J. A., Goldan, P. D., Kuster, W. C., Shao, M., Lovejoy, E. R.,

RO$_2$ measurements and O$_3$ production during TexAQS 2006

R. Sommariva et al.

Title Page

Abstract | Introduction

Conclusions | References

Tables | Figures

|◄ | ►|

◄ | ►

Back | Close

Full Screen / Esc

Printer-friendly Version

Interactive Discussion

Fall, R., and Fehsenfeld, F. C.: Online volatile organic compound measurements using a newly developed proton-transfer ion-trap mass spectrometry instrument during New England Air Quality Study-Intercontinental Transport and Chemical Transformation 2004: performance, intercomparison, and compound identification, Environ. Sci. Technol., 39, 5390–5397, 2005. 23116

Wood, E. C., Herndon, S. C., Onasch, T. B., Kroll, J. H., Canagaratna, M. R., Kolb, C. E., Worsnop, D. R., Neuman, J. A., Seila, R., Zavala, M., and Knighton, W. B.: A case study of ozone production, nitrogen oxides, and the radical budget in Mexico City, Atmos. Chem. Phys., 9, 2499–2516, doi:10.5194/acp-9-2499-2009, 2009. 23129

Table 1. Average sensitivity index (Eq. 6) for *Prod(*O$_3$*)*, *Loss(*O$_3$*)* and *Net(*O$_3$*)*.

Parameter	*Prod(*O$_3$*)*	*Loss(*O$_3$*)*	*Net(*O$_3$*)*
NO	1	–	0.89
O$_3$	–	1	0.11
HO$_2$+ΣRO$_2$	1	0.18	0.90
k_{HO_2+NO}	0.36	–	0.32
k_{RO_2+NO}	0.63	–	0.57
$k_{HO_2+O_3}$	–	0.18	0.01
$j(O^1D)$	–	0.75	0.09
HO$_2$/(HO$_2$+ΣRO$_2$)	0.02	0.18	0.03
OH	–	0.07	0.01

Fig. 1. CO, CH$_4$ and VOC (ethane shown as an example) chemistry at high NO$_x$.
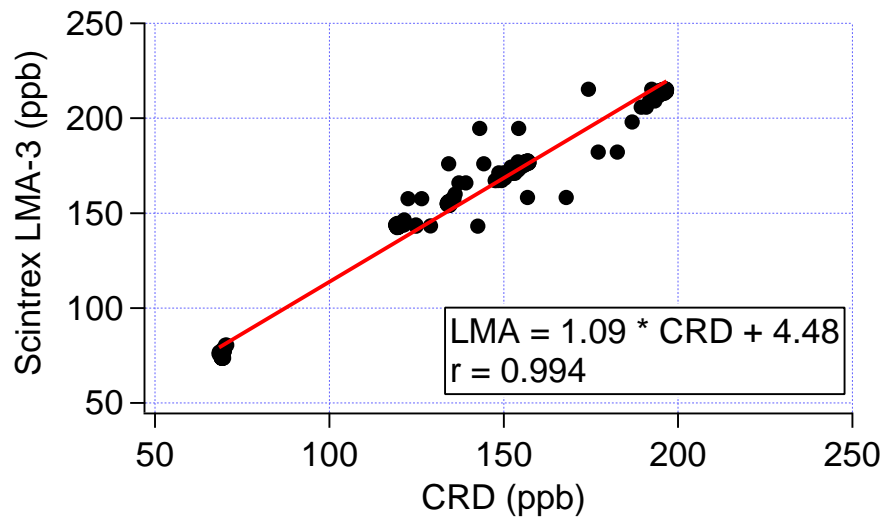
Fig. 2. Comparison between the Scintrex LMA-3 detector and the Cavity Ring-down Spectrometer during an NO_2 calibration of the PERCA instrument.
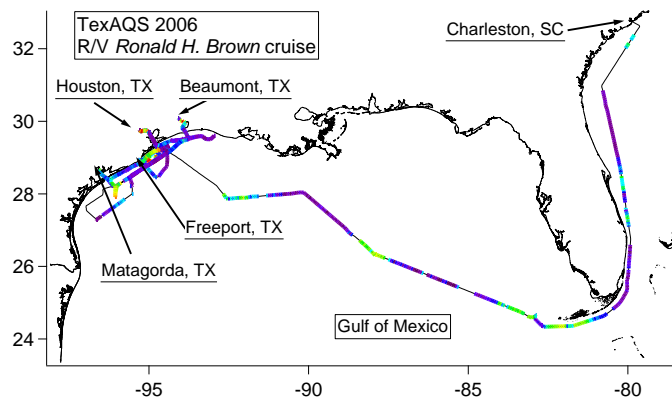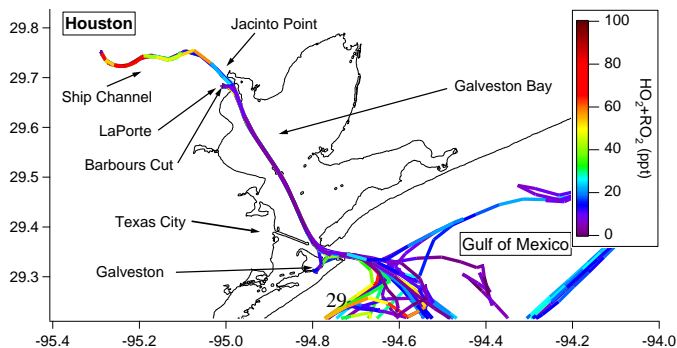
Fig. 3. Map of the Southern United States and the Gulf of Mexico showing the track of the R/V *Brown* during TexAQS 2006. The ship track is color-coded with $HO_2 + \Sigma RO_2$ measurements (in ppt). Note that several transects overlap, especially in the Galveston Bay and in the Houston Ship Channel, and that mixing ratios larger than 100 ppt are not shown.
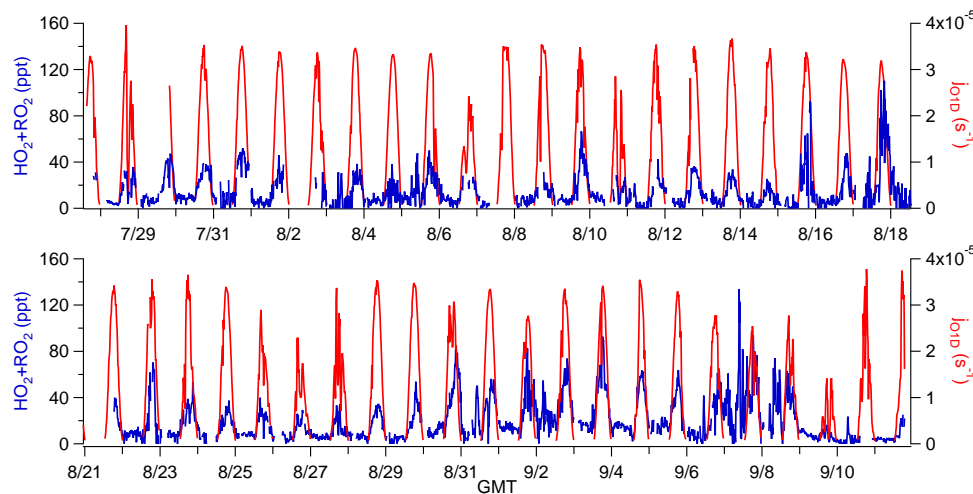
Fig. 4. Measurements of HO$_2$+ΣRO$_2$ (in blue) and j(O^{1}D) (in red) during the R/V *Brown* cruise.
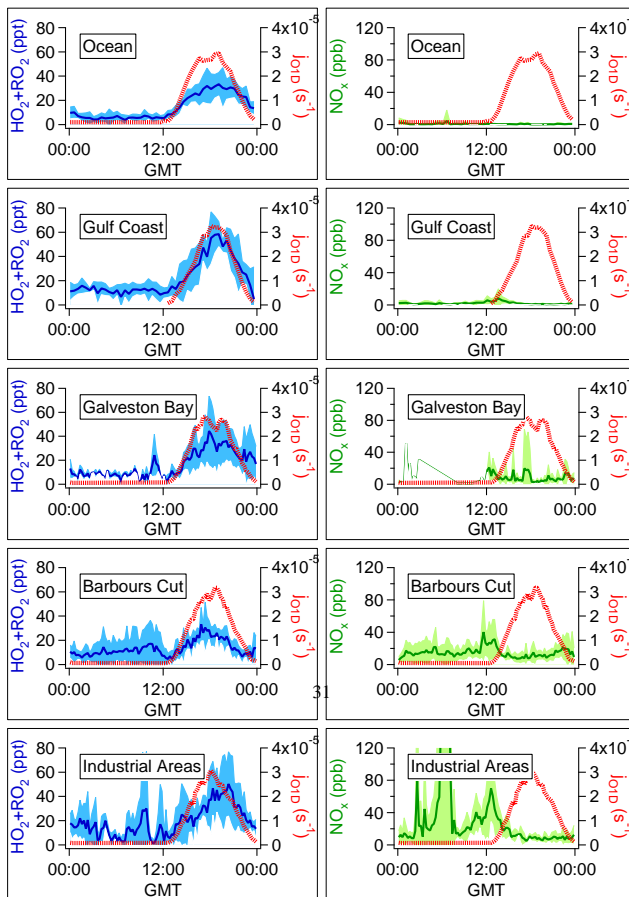
Fig. 5. Average diurnal profiles of $HO_2+\Sigma RO_2$ (in blue), NO_x (in green) and $j(O^1D)$ (in red) at different locations during the R/V *Brown* cruise. The shading corrsponds to 1-σ.
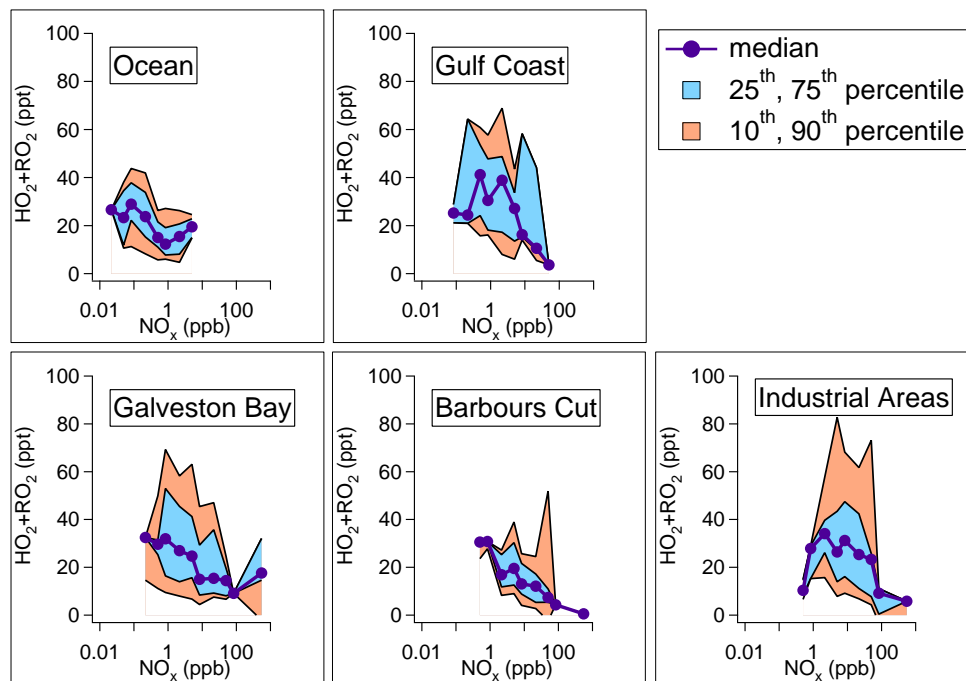
Fig. 6. Day-time measurements of $HO_2 + \Sigma RO_2$ vs. NO_x at different locations during the R/V *Brown* cruise.

Discussion Paper | Discussion Paper | Discussion Paper | Discussion Paper

ACPD

10, 23109–23147, 2010

RO$_2$ measurements and O$_3$ production during TexAQS 2006

R. Sommariva et al.

Title Page

Abstract	Introduction
Conclusions	References
Tables	Figures

|◄ | ►|

◄ | ►

Back | Close

Full Screen / Esc

Printer-friendly Version

Interactive Discussion
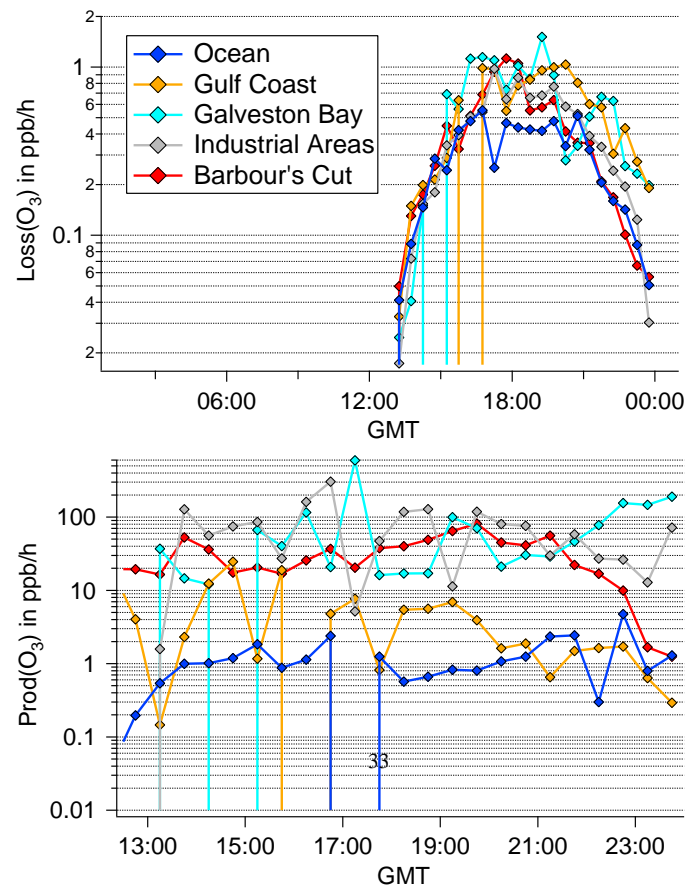
Fig. 7. Median diurnal profiles of *Loss(*O$_3$*)* and *Prod(*O$_3$*)* at different locations during the R/V *Brown* cruise.
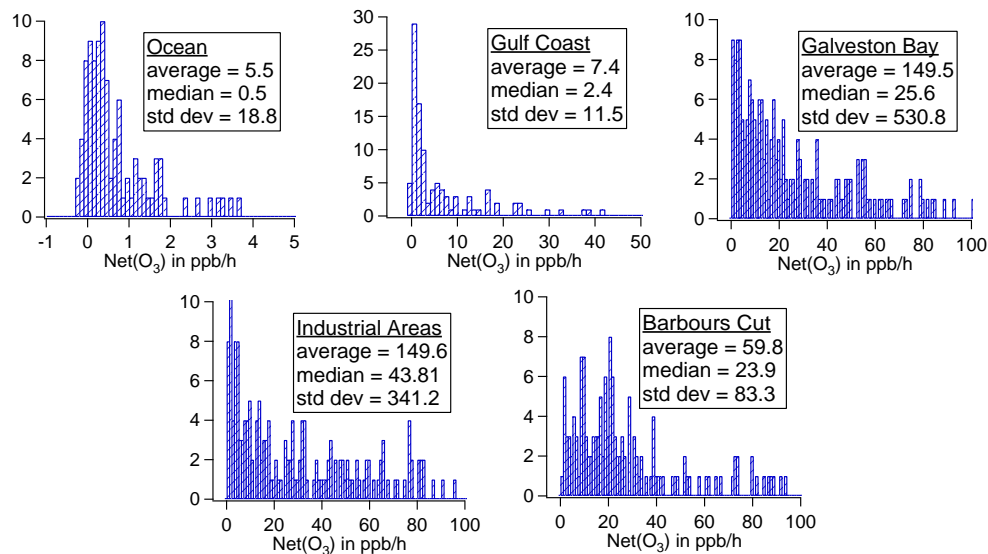
Fig. 8. Frequency distributions of *Net(*O$_3$*)* at different locations during the R/V *Brown* cruise. The bin size is 0.1 ppb/h for Ocean and 1 ppb/h for all the other locations. The values on the *y*-axis are the number of data points in each bin.

Discussion Paper | Discussion Paper | Discussion Paper | Discussion Paper | Discussion Paper

Title Page

Abstract | Introduction

Conclusions | References

Tables | Figures

|◄ | ►|

◄ | ►

Back | Close

Full Screen / Esc

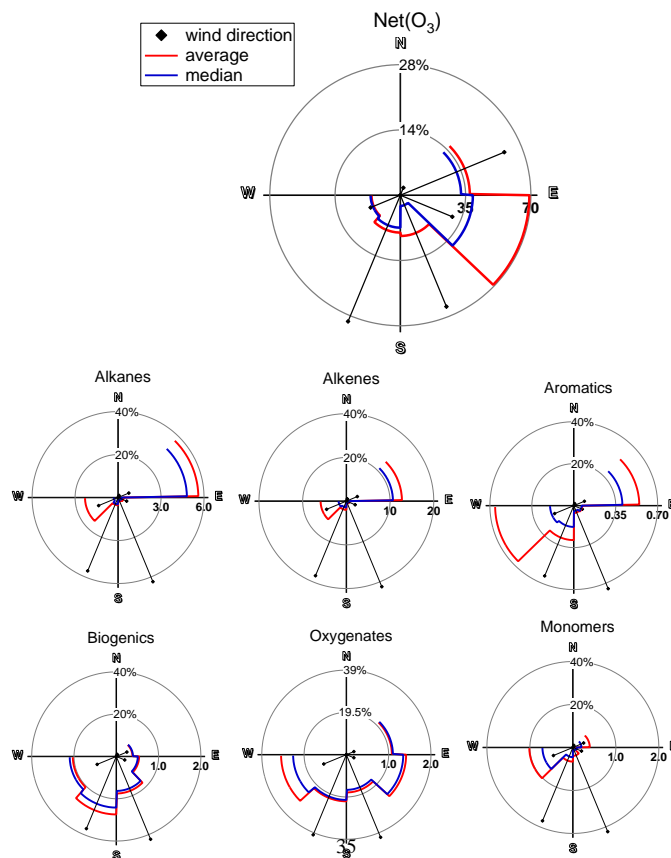Printer-friendly Version

Interactive Discussion

Fig. 9. *Net(*O_3*)* (in ppb/h) and OH reactivity of VOC classes (in s^{-1}) as function of local wind direction in Barbours Cut during TexAQS 2006. The values on the *x*-axis are the medians (blue) and the averages (red); the values on the *y*-axis indicate the frequency of the wind direction.

Title Page

Abstract | Introduction

Conclusions | References

Tables | Figures

|◄ | ►|

◄ | ►

Back | Close

Full Screen / Esc

Printer-friendly Version

Interactive Discussion
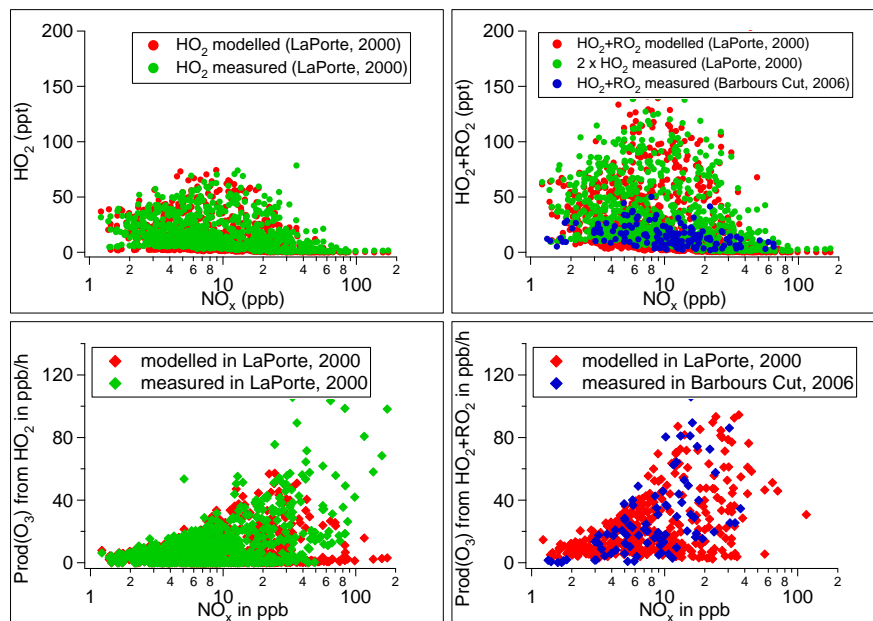
Fig. 10. Comparison of calculated and measured HO$_2$, HO$_2$+ΣRO$_2$ and *Prod(*O$_3$*)* in La-Porte (2000) and Barbours Cut (2006).